GeoAmericas2020
4th PAN AMERICAN CONFERENCE ON GEOSYNTHETICS
26-29 APRIL 2020 • RIO DE JANEIRO • BRAZIL

Numerical modeling of aggregate-geogrid composite behavior for pavement applications using Discrete Element Method

R. Borela, GSI Fellow, School of Computational Science and Engineering, Georgia Institute of Technology, Atlanta, USA
S. Hanumasagar, GSI Fellow, School of Civil and Environmental Engineering, Georgia Institute of Technology, Atlanta, USA
J. D. Frost, School of Civil and Environmental Engineering, Georgia Institute of Technology, Atlanta, USA
M. Wayne, Tensar International Corporation, Alpharetta, USA

ABSTRACT
The use of geogrids in road construction has been shown to augment service life and reduce aggregate consumption in pavement base layers (Montanelli et al., 1997). The enhanced performance arises from the lateral confinement of aggregates within geogrid apertures and improved granular interlocking (Giroud et al., 1985). The properties of aggregate-geogrid composite systems are influenced by gradation, aggregate morphology, geogrid stiffness, aperture shape and size, among others (Giroud and Han, 2004). The present study examines effects of such factors on the cyclic-loading behavior of geogrid-stabilized base layers using the discrete element method. Three-dimensional models simulated 3 stabilization conditions (non-stabilized, triaxial geogrid and full lateral confinement) for 3 diameter-to-rib length ratios. Aggregates were modeled as mono-sized spheres interacting via an elasto-plastic frictional contact law (Cundall and Strack., 1979), and geogrids followed a deformable element formulation (Effeindzourou et al., 2016). Stabilization cases proposed in this study offer a new and improved framework for assessing aggregate-geogrid systems based on rutting performance as follows. The upper and lower bounds are established by the non-stabilized and the full lateral confinement cases, respectively. In the latter, horizontal motion is fully constrained within a thin layer of aggregate elements while maintaining free vertical movement. This represents an idealized system where particles near the geogrid are completely laterally restrained. Results show an evolution of the composite response according to different diameter-to-rib-length size ratios in relation to the upper and lower bound cases.

1. INTRODUCTION

The use of geogrids for pavement applications has proved advantageous in reducing the permanent deformation resulting from cyclic loading over the lifecycle of a pavement (Montanelli et al., 1997; Giroud et al., 1985). The reduction of permanent deformation is a direct result of the lateral confinement provided by the interlocking between the geogrid and surrounding aggregate, which is influenced by an array of factors relating the geogrid morphology and size as well as the geogrid aperture size and shape (Giroud and Han, 2004). In addition to the vast literature on experimental work on this topic, various studies have concentrated on the numerical modeling of geogrids using the discrete element method (DEM) in three dimensions.
Different techniques have been utilized to model geogrids, considering them as rigid elements in Tutumluer et al. (2010) and Qian et al (2011), as well as deformable elements in Stahl et al. (2013), Ngo et al. (2014) and Effeindzourou et al. (2016). These efforts have been successful at capturing the geogrid-aggregate interaction; however, these have focused solely on investigating the performance of non-stabilized specimens in comparison to their stabilized counterparts.
The objective of the present study was to establish a new modelling framework by which the performance of geogrids can be evaluated in order to optimize their application, as well as guide the design of new technologies. The numerical model cyclic loading of pavement layers subject to different stabilization conditions based on the discrete element method (DEM) developed in this study, enabled an evaluation within the potential range of improvement that can be achieved using geogrid stabilization

2. METHODOLOGY

The discrete element method is well suited for the objectives of this study as it enables insight into the aggregate-geogrid kinematics at the particulate level. The modeling approach consisted of the following steps. First, an appropriate constitutive law for aggregate-aggregate contacts and an explicit formulation for the geogrid geometry and behavior were selected. Input parameters for the geogrid model were calibrated using experimental data. Aggregate base layer specimens were then generated numerically and subjected to cyclical loading by a cylindrical piston. The model was developed using the open-source software YADE (Šmilauer et al., 2015).

2.1 Model formulation and calibration

Base layer aggregates were represented as spherical elements interacting via the elasto-frictional law proposed by Cundall and Strack (1979), in which the contact between elements offers both to normal and frictional resistance. The geogrid was modeled as a deformable material using the formulation developed by (Effeindzourou et al., 2016). Since in reality the ribs are expected to withstand only low compressive forces before buckling, ribs were generated with an articulated node at mid-length to mitigate potential artifacts arising from excessive resistance under compression. The geometry of the ribs was approximated by cylinders of cross-sectional area equivalent to that of the reference physical grid rib. The ribs worked in axial compression and extension, as well as in bending and torsion. The surface of the ribs, defined by the Minkowski sum between corresponding grid nodes, was assigned the same contact law as that used for the aggregate-aggregate contacts. The subgrade and loading piston were both modeled as rigid facets, with elastic frictionless contacts with the aggregates.
The triaxial geogrid TX190L manufactured by Tensar Corp was selected as the reference material for the model. The geogrid geometry consists of equilateral triangles of rib length of 6 cm. Based on the previously described geogrid formulation, the following parameters were calibrated: rib axial stiffness, nodal bending and torsional stiffness, normal and shear strength.
The ASTM standard tests for rib stiffness (D6637/D6637M-15) and for out-of-plane stiffness (D7748/D7748M-14e1) were replicated numerically. First, a series of simulations in which a single rib was axially strained were conducted, adjusting the axial stiffness property iteratively until results matched the experimental characterization. Once the axial stiffness was calibrated, the out-of-plane stiffness test was modeled. A section of the geogrid spanning two triangular openings in width was hung from a surface, with a cantilever length equivalent to that obtained during the physical characterization. The bending and torsional stiffness were then adjusted until the tip of the geogrid strip formed a 45° angle with the horizontal plane, as prescribed in (D7748/D7748M-14e1). The test apparatus is illustrated in Figure 1a.

2.2 Base layer specimen generation

The sample generation procedure is selected to generate specimens using a similar compaction method as that employed in the field. First a loose cloud of spheres is generated and compacted using multiple cycles of oedometric displacement-controlled loading/unloading. The specimen is then allowed to reach dynamic balance under gravity. On the horizontal boundaries, periodic boundary (O'Sullivan, 2011) conditions were employed. The lower boundary consists of a rigid plate. In both non-stabilized and geogrid stabilized cases, with the final base thickness corresponding to 25 cm ± 1 cm and a porosity in the 41% – 46% range. The diameter-to-rib-length ratio of an inscribed sphere in the triangular opening corresponds to approximately 0.57, defining the threshold for an element to fit through the grid. Therefore, the grid may produce a degree of separation between upper and lower layers in stabilized specimens generated with diameter-to-rib-length ratios larger than the threshold. In turn effecting an increased porosity when compared to their non-stabilized counterparts. A total of 6 specimens were generated consisting of one stabilized and one non-stabilized specimen for each of three different diameter-to-rib-length ratios. A sample stabilized specimen with the loading piston is presented in Figure 1b.

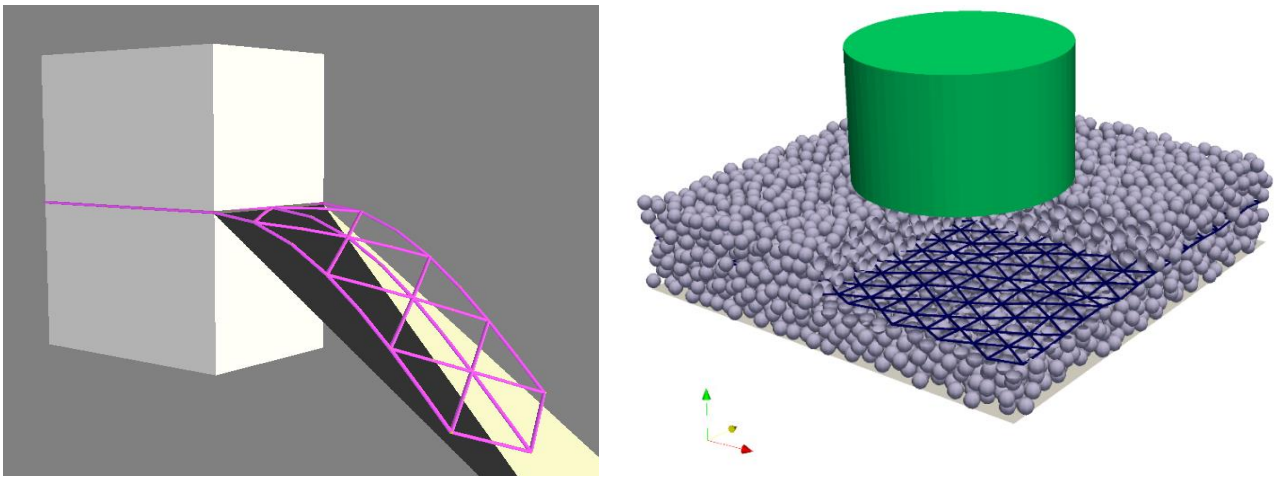

a) Calibration of geogrid model by flexural rigidity test b) Sample specimen with piston before cyclic loading test

Figure 1. Illustrations of grid calibration procedure and grid stabilized specimen

2.3 Cyclic loading

After the specimens were generated, they were subjected to cyclic loading by a cylindrical piston. The load application was performed using a PID controlled system (Šmilauer et al., 2015). In this control scheme, the piston was translated in the vertical direction to maintain the target load pressure during loading and a sitting pressure during the unload cycle. The target pressure was set at 275.8 kPa, while the seating pressure was set at 10% of that of loading, at 27.6 kPa. Loading was applied at a frequency of 50 Hz, in which the loading and unloading phases had the same duration as shown in Figure 2a.
In the specific case of the fully lateral confinement models, a thin layer of aggregate elements in the specimen had their movement in the xy plane constrained to zero while maintaining their free vertical movement, as illustrated in Figure 2b. This represents the lower bound for rutting (Figure 2c), equivalent to an idealized aggregate-geogrid system where particles near the geogrid are completely laterally restrained.

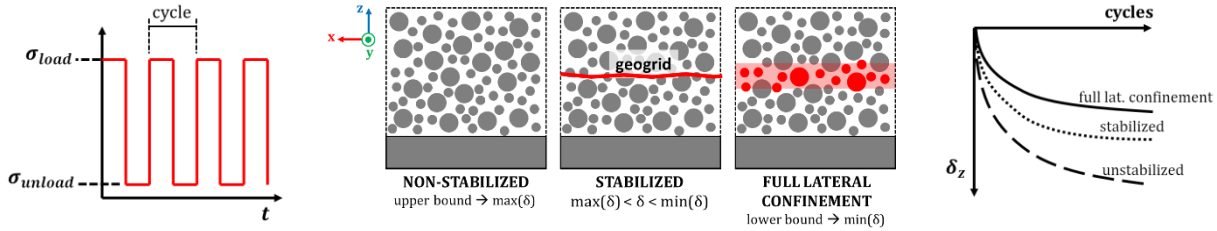

a) Input loading cycle b) Stabilization conditions c) Theoretical rutting behavior

Figure 2. Framework for evaluating geogrid performance

By obtaining knowledge of the maximum improvement to be expected solely based on lateral confinement (lower rutting bound), the full range of performance improvement can be quantified, providing more meaningful information concerning the aggregate-geogrid composite behavior. The surface displacement ratio can then be defined as expressed in Equation 1, where δ corresponds to rutting at a given loading cycle for different stabilization cases.

$$Surface\ displacement\ ratio = \frac{\delta_{stabilized} - \delta_{non-stabilized}}{\delta_{full\ lat.\ confinement} - \delta_{non-stabilized}} \quad [1]$$

This index ratio is defined on the interval between 0 and 1. The surface displacement ratio has a value of 1, when the stabilized layer behaves close to the idealized form (full lateral confinement) and a value 0 when the interlocking between aggregate and geogrid does not provide any significant lateral confinement.

3. RESULTS AND DISCUSSION

Figures 3, 4 and 5 show the results of simulations corresponding to a specimen subjected to 200 load cycles, for 9 cases: 3 stabilization conditions for 3 aggregate diameter-to-rib-length ratios (0.7, 0.5 and 0.3). The evolution in porosity was tracked in a cuboidal region circumscribed by the piston base over the height of the underlying specimen. The rutting was measured at the center of the loading piston base. It can be observed that in all cases the geogrid had an impact improving the rutting performance of the specimens. Figure 6 displays the surface displacement ratio as defined by Equation 1, providing insight into the different trends observed with the 3 different diameter-to-rib-length ratios. A review of the results presented in Figures 3 to 7 reveal the following insights:

- In the specimen with a size ratio of 0.7 the performance at the start is close to the idealized case, the performance then degrades with continuous cyclic loading. By investigating the kinematic behavior of the system in Figures 7a-c, it becomes evident that the geogrid is moving along with the particles and the observed rutting improvement is mostly the result of the geogrid carrying part of the load from the piston. This is further corroborated by the fact that the stabilized and non-stabilized curves are parallel with increasing load cycles. This is a consequence of the large particle size in comparison to the openings in the geogrid preventing proper interlocking.
- For the specimen with a size ratio of 0.5, the improvement in the performance is relatively constant throughout the test. Figures 7d-f reveal that the geogrid helped reduce the displacement significantly, effectively providing confinement to the specimen.
- Finally, for the specimen with a size ratio of 0.3, an increase in the performance is observed over time. By observing Figures 7g-i, it can be observed that the geogrid provides an important degree of confinement, however this effect takes place at a much higher loading cycle. This indicates that a significant amount of compaction takes place before the geogrid interlocking effect can be observed on the specimen macro-response.

Finally, the rutting observed for all cases in (Figures 3 to 5) is quite significant considering the height of the specimens. Based on Figures 7a-I, it becomes evident that particles experience considerable displacements in non-stabilized and stabilized cases. This can be attributed to the spherical shape and elasto-frictional contacts, which do not offer comparable constraint to that of non-spherical aggregates, in which rolling would be more readily impeded. Therefore, despite reaching a terminal porosity in early cycles, rutting continues to increase due to the compound effect of small slips at particle contacts.

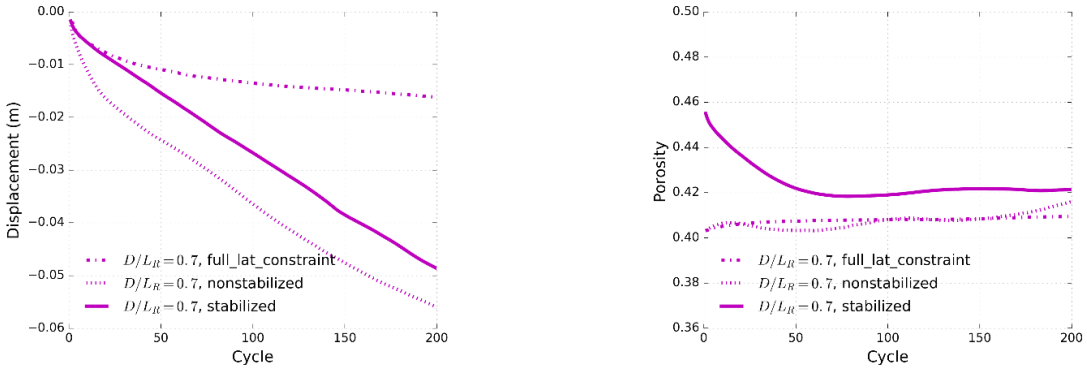

a) Rutting evolution over loading cycles

b) Porosity evolution over loading cycles

Figure 3. Rutting and porosity behavior of specimen with size ratio of 70% for different stabilization conditions

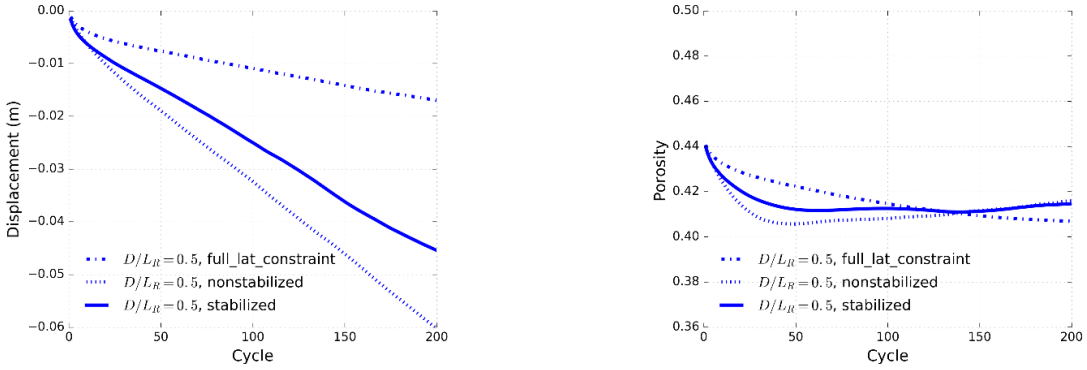

a) Rutting evolution over loading cycles

b) Porosity evolution over loading cycles

Figure 4. Rutting and porosity behavior of specimen with size ratio of 50% for different stabilization conditions

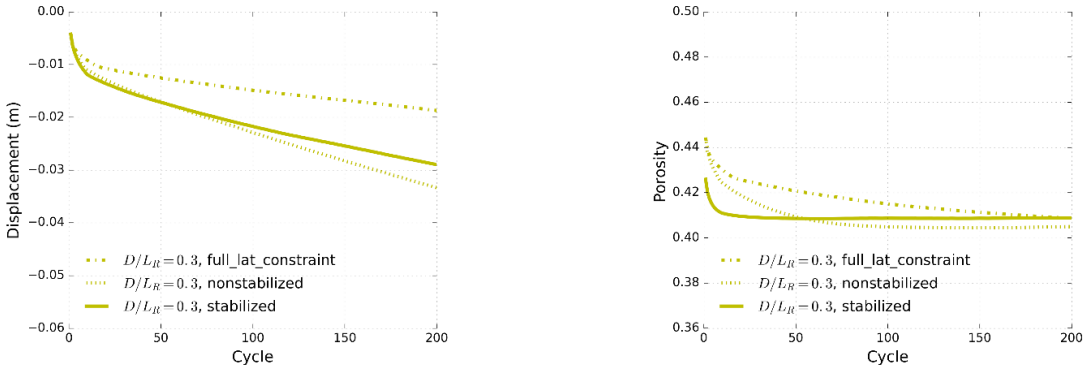

a) Rutting evolution over loading cycles

b) Porosity evolution over loading cycles

Figure 5. Rutting and porosity behavior of specimen with size ratio of 30% for different stabilization conditions

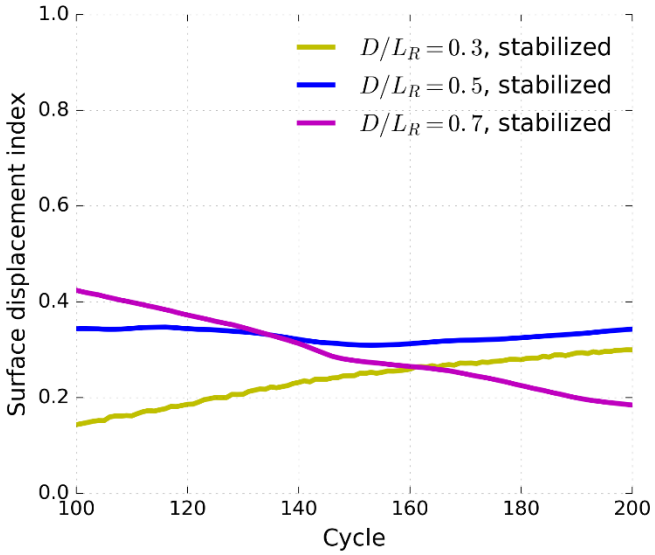

Figure 6. Surface displacement ratio for different size ratios from cycle 100 to 200.

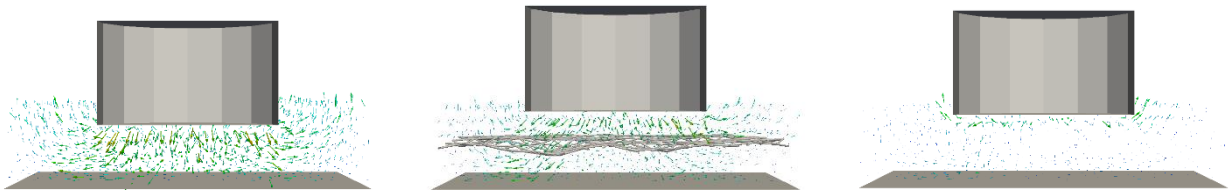

a) Non-stabilized, size ratio = 70% b) Stabilized, size ratio = 70% c) Full lat. confined, size ratio = 70%

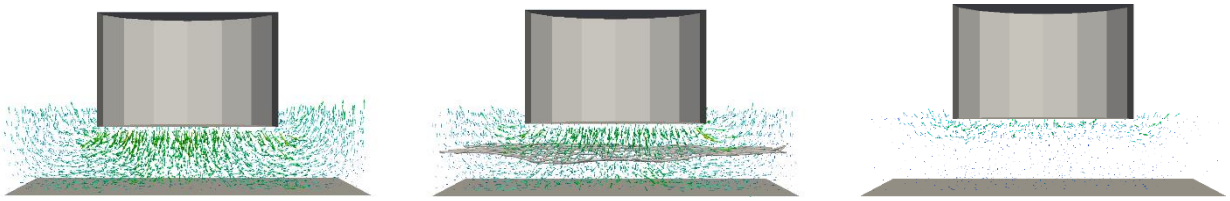

d) Non-stabilized, size ratio = 50% e) Stabilized, size ratio = 50% f) Full lat. confined, size ratio = 50%

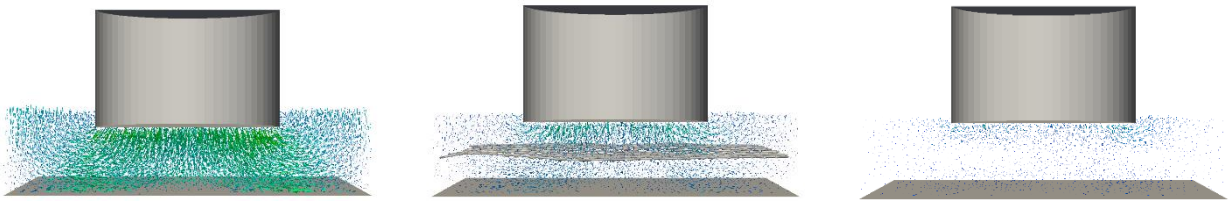

g) Non-stabilized, size ratio = 30% h) Stabilized, size ratio = 30% i) Full lat. confined, size ratio = 30%

Figure 7. Profile of aggregate displacement field at 100 loading cycles for different aggregate sizes and stabilization conditions.

4. FINAL CONSIDERATIONS

A new framework for evaluating geogrid performance has been presented in this paper with an application example. By employing the discrete element method, it is possible to obtain a better understanding of the range of performance of a

geogrid stabilized base layer. These can lead to the development of better usage guidelines that optimize the composite aggregate-geogrid behavior.
It is important to note that aggregate base layers are composed mainly of crushed stone, characterized by high angularity and non-sphericity (Kwon et al., 2014). These morphological features give rise to tight interlocking between grains and result in a stiff granular matrix. The current modeling approach with spherical elements and an elasto-frictional contact law does not fully capture these aspects.
As noted in the literature, the morphological characteristics of the aggregates play an important role in the composite behavior, such that the optimal aggregate diameter-to-rib-length ratio will change for different degrees of angularity. The current model is being extended to include such effects with an additional suite of simulations.

ACKNOWLEDGEMENTS

The study presented herein has been supported by the School of Civil and Environmental Engineering at the Georgia Institute of Technology, Tensar Corporation and student fellowships provided by the Geosynthetics Institute to the first two authors.

REFERENCES

ASTM D6637/D6637M-15, Standard Test Method for Determining Tensile Properties of Geogrids by the Single or Multi-Rib Tensile Method, *American Society for Testing and Materials*, West Conshohocken, Pennsylvania, USA.

ASTM D7748/D7748M-14e1, Standard Test Method for Flexural Rigidity of Geogrids, Geotextiles and Related Products, , *American Society for Testing and Materials*, West Conshohocken, Pennsylvania, USA.

Cundall, P. A. and Strack, O. D. L. (1979), A discrete numerical model for granular assemblies, *Géotechnique* 29(1): 47-65.

Effeindzourou, A., Chareyre, B., Thoenia, K., Giacomini, A., Kneib, F. (2016) Modelling of deformable structures in the general framework of the discrete element method*, Geotextiles and Geomembranes*, 44(2):143-156.

Giroud, J., et al., (1985), Design of unpaved roads and trafficked areas with geogrids. *Polymer grid reinforcement*, Thomas Telford Publishing, 116-127.

Giroud, J. and Han, J., (2004), Design method for geogrid-reinforced unpaved roads. I. Development of design method, *Journal of Geotechnical and Geoenvironmental Engineering*, 130(8): 775-786.

Kwon, J., Boudreau, R. L., Tutumluer, E. and Wayne, M. H., (2014), Evaluation and Characterization of Aggregates for Sustainable Use in Pavement Engineering, *Geo-Congress 2014*, ASCE, Atlanta, GA, USA, 1:3373-3382.

Montanelli, F., Zhao, A. and Rimoldi, P., (1997), Geosynthetic-reinforced pavement system: testing and design. *Geosynthetics '97, TRB,* Long Beach, California, USA, 1:619-632.

Ngo, N. T., et al., (2014), DEM simulation of the behavior of geogrid stabilized ballast fouled with coal. *Computers and Geotechnics,* 55: 224-231.

O'Sullivan, C., (2011), *Particulate discrete element modelling*, 1st ed., CRC Press, London, UK.

Qian, Y., et al., (2011), A validated discrete element modeling approach for studying geogrid-aggregate reinforcement mechanisms. *Geo-Frontiers Congress 2011*, ASCE, Dallas, TX, USA, 1:4653-4662.

Šmilauer, V. et al., (2015), Yade Documentation 2nd ed. The Yade Project. DOI 10.5281/zenodo.34073 (http://yade-dem.org/doc/).

Stahl, M., et al., (2014), Discrete element simulation of geogrid-stabilized soil. *Acta Geotechnica* 9(6): 1073-1084.

Tutumluer, E., et al, (2010), Geogrid-Aggregate interlock mechanism investigated through aggregate imaging-based discrete element modeling approach, *International Journal of Geomechanics* 12(4): 391-398.